Rate Coefficients for the Reactions of OH and OD with HCl and DCl between 200 and 400 K

Frédérique Battin-Leclerc,[†] In Koo Kim,[‡] Ranajit K. Talukdar, Robert W. Portmann,[‡] and A. R. Ravishankara*,[‡]

National Oceanic and Atmospheric Administration, Aeronomy Laboratory, Boulder, Colorado 80303, and The Cooperative Institute for Research in Environmental Sciences, University of Colorado, Boulder, Colorado 80309

Rozeanne Steckler and Danielle Brown

San Diego State University and San Diego Supercomputer Center, P.O. Box 85608, San Diego, California 92186

Received: January 12, 1999; In Final Form: March 2, 1999

Rate coefficients for the reaction of OH radical with HCl (k_1) between 200 and 400 K, were measured to be $3.28 \times 10^{-17}\ T^{1.66} \exp[184/T]$ cm^3 molecule^{-1} s^{-1} by producing OH via pulsed laser photolysis and detecting it via laser induced fluorescence. The rate coefficients for the reactions of OH with DCl (k_2), OD with HCl (k_3), and OD with DCl (k_4) were also measured using the same method to be $k_2 = 2.9 \times 10^{-12} \exp[-728/T]$, $k_3 = 8.1 \times 10^{-18}\ T^{1.85} \exp[300/T]$, and $k_4 = 2.5 \times 10^{-12} \exp[-660/T]$ cm^3 molecule^{-1} s^{-1}. $k_1 - k_4$ were computed for $200 < T < 400$ K using the variational transition theory, including tunneling corrections, to be $k_1 = 1.49 \times 10^{-16}\ T^{1.35} \exp[262/T]$, $k_2 = 9.04 \times 10^{-20}\ T^{2.34} \exp[429/T]$, $k_3 = 1.01 \times 10^{-16}\ T^{1.4} \exp[309/T]$, and $k_4 = 1.64 \times 10^{-19}\ T^{2.27} \exp[385/T]$cm^3 molecule^{-1} s^{-1}, in reasonable agreement with experiments. They were also used to analyze the origin of the isotope effects. A two-dimensional chemical transport model calculation shows that our measured higher values of k_1 at low temperatures do not significantly alter the calculated ozone abundance, or its trend, in the stratosphere.

Introduction

HCl is a principal reservoir of inorganic chlorine in the stratosphere. Many processes, including heterogeneous reactions, gas-phase free radical reactions, and photolysis, convert HCl to active forms that take part in catalytic ozone destruction cycles. Heterogeneous conversion of HCl to active Cl is important below ∼210 K, i.e., in the lower stratosphere. Free radical reactions dominate at warmer temperatures, i.e., in the mid to upper stratosphere. Photolysis is important only in the upper stratosphere. The OH radical is the major free radical responsible for converting HCl to Cl in the stratosphere via the reaction:

$$OH + HCl \rightarrow H_2O + Cl; \quad k_1 \qquad (1)$$

The most recent evaluation[1] of k_1 is based on the measurements of Molina et al.[2] (from 240 to 295 K), Keyser[3] (from 258 to 334 K), and Ravishankara et al.[4] (from 240 to 1055 K). However, measurements by Sharkey and Smith,[5] in the temperature range 138−298 K, disagree significantly with this recommendation below ∼220 K. Further, Sharkey and Smith report k_1 to be nearly independent of temperature below 216 K. Calculations by Steckler et al.[6] also suggest that the recent evaluation of k_1 is not accurate at low temperatures. This study aims to resolve the discrepancy at low temperature, and to explore the origin of the curvature in the Arrhenius plot. To understand the mechanism of the reactions and to ensure that the measured k_1 values were not influenced by systematic errors, the temperature-dependent rate coefficients were also measured and calculated for the following H/D isotopic variation of reaction 1:

$$OH + DCl \rightarrow HOD + Cl; \quad k_2 \qquad (2)$$

$$OD + HCl \rightarrow HOD + Cl; \quad k_3 \qquad (3)$$

$$OD + DCl \rightarrow D_2O + Cl; \quad k_4 \qquad (4)$$

The implications of the measured rate constants to the changes in stratospheric ozone abundance are also explored using a numerical two-dimensional atmospheric model.

Experiments and Results

OH radicals were produced via pulsed photolysis of a suitable precursor (HNO_3 or H_2O_2) and detected by pulsed laser-induced fluorescence (PP−PLIF). The details of the apparatus, data acquisition methodology, and data analysis are given elsewhere.[7] Therefore, we will only describe the essentials needed to understand the present experiments.

A 150 cm^3 jacketed Pyrex cell was maintained at a constant temperature by flowing methanol or ethylene glycol from a thermostated cooling or heating bath. The temperature in the reaction zone, defined by the intersection between the photolysis and the probe laser beams, was measured by a retractable

[†] Departement de Chimie-Physique des Reactions, ENSIC, CNRS, 1, Rue Grandville- B. P. 451 F 54001, Nancy Cedex, France

[‡] Also associated with the Department of Chemistry and Biochemistry, University of Colorado, Boulder, CO 80309.

10.1021/jp990177j CCC: $18.00
Published on Web 04/29/1999

thermocouple. The measured temperature was constant to within ±1 K and known to better than 0.5 K.

Gas mixtures containing the OH(OD) precursor, HCl or DCl, and ultrahigh purity (UHP) helium (in some cases SF_6) were flowed through the reaction cell. All the gas flows, except that of HCl (DCl), were measured by calibrated electronic mass flow meters. The concentrations of HCl and DCl were measured by 184.9 nm (Hg pen ray lamp) absorption in 100 cm long absorption cells located both before and after the reactor. The absorption cross section of HCl/DCl at 184.9 nm was determined by measuring the absorbance of manometrically prepared 1−3% mixtures of HCl/DCl in He at different pressures in a 100 cm cell. The measured absorption cross sections were $\sigma_{184.9}^{HCl} = (3.26 \pm 0.10) \times 10^{-19}$ cm^2 molecule^{-1} $\sigma_{184.9}^{DCl}$ and $= (2.96 \pm 0.12) \times 10^{-19}$ cm^2 molecule^{-1}. The measured HCl cross section agrees to within 4% with the literature value.[1] To our knowledge, the absorption cross section of DCl has not been previously reported.

The pressure in the reaction cell was maintained between 50 and 100 Torr. The gas flow velocities through the reaction zone were 10−20 cm s^{-1}, sufficient to replenish this volume with a fresh gas mixture between laser pulses (operating at 10 Hz). Some of the measurements were performed at a flow velocity of 5 cm s^{-1} to check the effect of flow velocity on the measured rate coefficients.

Reactions 1−4 were studied under pseudo-first-order conditions in OH/OD. Under these conditions, the temporal profiles of OH/OD followed the equation:

$$[OX]_t = [OX]_0 \exp(-k^I t) \quad \text{(I)}$$

$$k^I = k_i[XCl] + k_d \quad \text{(II)}$$

where X = H or D, k_i refers to the rate coefficient of reactions 1−4, and k_d is the first-order rate coefficient for the loss of hydroxyl radical (OH or OD) in the absence of HCl and DCl.

The temporal profiles of OH/OD were fit to eq I using nonlinear least-squares analyses to calculate the first-order rate coefficients k^I. The values for k_i were obtained by fitting k^I vs [HCl] or [DCl] data to eq II using linear least-squares analysis. In these experiments, k^I was 10−70 times larger than k_d. Therefore, small fluctuations (<10%) in k_d, due to the variations in the OH/OD precursor concentrations during the measurement of k^I values at various HCl/DCl concentrations, did not affect the obtained value of k_i.

To identify systematic errors, the following sources of OH were used: (1) HONO photolysis at 355 nm (third harmonic of a Nd:YAG laser), (2) photolysis of HNO_3 at 248 nm (KrF excimer laser), and (3) photolysis of H_2O_2 at 248 nm (KrF excimer laser). The OD radicals were always generated via 248 nm photolysis of DNO_3. The concentrations of the OH (OD) precursor were varied between 5×10^{13} and 5×10^{14} molecules cm^{-3} in different experiments to measure k_1 and k_4. To minimize isotope exchange while measuring k_2 and k_3, the concentrations of OH (OD) precursors were maintained below 5.0×10^{13} molecule cm^{-3}. The concentrations of HNO_3 /DNO_3 in the gas mixture flowing through the cell were directly measured by absorption of 184.9 nm (from a Hg pen ray lamp) in a 100 cm absorption cell located before the point where DCl/HCl was introduced into the gas flow. The absorption cross section for HNO_3, $\sigma_{184.9}^{HNO_3} = 1.58 \times 10^{-17}$ cm^2 molecule^{-1}, was taken from the NASA/JPL evaluation.[1] The absorption cross section for DNO_3 was assumed to be same as that for HNO_3. Upper limits for the concentrations of H_2O_2 and HONO, which were not directly measured, were estimated by attributing the measured first-order loss rate coefficient of OH in the absence of HCl/DCl entirely to their reactions. The OH/OD concentrations, calculated from the concentrations of the corresponding precursors, their absorption cross sections at the photolysis wavelengths, and the photolysis laser fluence, were always $< 5 \times 10^{11}$ molecule cm^{-3}.

HCl, from Scott Specialty Gases (purity >99.995%) and DCl from Cambridge Isotope Laboratories (chemical purity >99.99%, >99% D), were stored in 12 L Pyrex bulbs. Ultrahigh purity He (>99.9995% purity), used as the bath gas, was obtained from U.S. Bureau of Mines. Instrument grade SF_6 (>99.99%) was obtained from Scott Specialty Gases. HNO_3 was prepared by reaction of concentrated H_2SO_4 with solid $NaNO_3$ and collected by vacuum distillation at 77 K. D_2SO_4 was added to the DNO_3 purchased from Cambridge Isotope Laboratories (66.3% in D_2O) to lower the vapor pressure of D_2O and thus minimize the possibility of condensation inside the Pyrex injector. It also helped convert any H_2O to D_2O. HONO was produced by dropwise addition of a 0.1 M solution of $NaNO_2$ to a 10% solution of H_2SO_4. The HONO source and DNO_3 container were maintained at 273 K (ice bath), while the HNO_3 container was kept at 250 K (mixture of ice and NaCl). The low temperature was necessary to better control the flow rates of the OH precursors.

In reactions 2 and 3, HNO_3 and DNO_3 were used as precursors of OH and OD. Exchange of H and D between HCl and DNO_3, and between DCl and HNO_3, will affect the measured values of k_2 and k_3. Since HCl and DCl are indistinguishable via UV absorption, formation of DCl from HCl or HCl from DCl will go unnoticed. Conversion of even a fraction of DCl to HCl would increase the measured value of k_2. In reaction 3, on the other hand, any conversion of HCl to DCl would decrease the measured value of k_3. When HNO_3 and DCl were flowed together in the system and allowed to interact for a significant time (seconds), there was indeed noticeable H to D exchange. For example, addition of $(1.3-11.5) \times 10^{16}$ molecule cm^{-3} of DCl into a gas flow containing $\sim 6 \times 10^{13}$ cm^{-3} of HNO_3 decreased the measured OH signal by 35−70%. Simultaneously, OD was produced when this mixture was photolyzed by 248 nm. These observations clearly indicate that the H/D exchange occurred between HNO_3 and DCl, presumably on the surface of the absorption cell and the reactor. To minimize isotope exchange between HCl and the OD precursor, as well as between DCl and the OH precursor, HNO_3/DNO_3 was introduced into the reactor through a Pyrex injector ~1 cm (interaction time <100 ms) above the reaction zone. This procedure also minimized exposure of the precursors to the walls of the reactors. In addition, the concentration of DNO_3/HNO_3 was kept so low ($\sim 5 \times 10^{13}$ molecule cm^{-3}) that a very small fraction of the HCl/DCl would have been converted even if all of DNO_3/HNO_3 had reacted with HCl/DCl. In this arrangement, sufficient DNO_3/HNO_3 was left in the reactor even when large concentrations (up to 10^{17} molecule cm^{-3}) of HCl/DCl was added such that OD/OH radical signal was essentially unaltered, demonstrating that isotopic exchange was minimal. However, with this arrangement, the mixtures of HNO_3 or DNO_3 in He had to be introduced into the reaction cell prior to dilution by the buffer gas. As a result, concentrations of DNO_3/HNO_3 had to be sufficiently high in the injector (a factor of 100 higher than in the reactor after mixing). Under these conditions a large fraction of the photolyte condensed in the injector at temperatures below ~250 K. Thus, we could measure k_2 and k_3 only at $T > 250$ K.

TABLE 1: Rate Coefficient for the Reaction of OH with HCl Reaction, k_1, and the Relevant Experimental Conditions for Their Measurements

temperature (K)	pressure (Torr)	buffer gas/ OH precursor	$[OH]_0$ (10^{10} cm^{-3})	[HCl] (10^{15} cm^{-3})	$(k_1 \pm \sigma^a) \times 10^{13}$ (cm^3 molecule^{-1} s^{-1})	$(k_1 \pm 2\sigma^b) \times 10^{13}$ (cm^3 molecule^{-1} s^{-1})
200	60	He/HNO_3	6	1.4−14.1	5.78 ± 0.05	5.78 ± 0.31
205	61	He, SF_6/HONO	44	0.8−5.3	5.47 ± 0.23	5.47 ± 0.54
211	61	He/HNO_3	6	1.5−12.7	5.91 ± 0.06	5.91 ± 0.32
212	51	He, SF_6/HONO	19	1.4−7.8	5.47 ± 0.22	5.47 ± 0.52
212	62	He, SF_6/HONO	40	1.1−7.0	5.92 ± 0.16	5.92 ± 0.42
212	83	He/HNO_3	1	1.4−12.6	5.94 ± 0.05	5.94 ± 0.31
222	60	He/HNO_3	7	1.6−13.1	6.02 ± 0.07	6.02 ± 0.33
224	63	He, SF_6/HONO	27	1.7−6.7	5.83 ± 0.12	5.83 ± 0.38
234	51	He, SF_6/HONO	9	1.2−9.8	6.68 ± 0.20	6.68 ± 0.52
234	62	He/HNO_3	7	1.1−10.1	6.42 ± 0.08	6.42 ± 0.36
243	61	He, SF_6/HONO	11	1.8−6.0	6.35 ± 0.14	6.35 ± 0.42
251	50	He, SF_6/HONO	11	0.7−8.7	6.65 ± 0.10	6.65 ± 0.39
254	60	He, SF_6/HNO_3	3	1.5−15.3	6.57 ± 0.13	6.57 ± 0.42
262	60	He/HNO_3	7	0.9−12.3	7.00 ± 0.07	7.00 ± 0.38
263	63	He, SF_6/HONO	20	1.6−7.8	6.71 ± 0.21	6.71 ± 0.54
277	62	He, SF_6/HONO	14	1.4−8.4	7.70 ± 0.24	7.70 ± 0.62
297	48	He, SF_6/HONO	9	0.7−2.9	7.74 ± 0.41	7.74 ± 0.91
299	62	He, SF_6/HNO_3	2	1.1−7.7	8.04 ± 0.15	8.04 ± 0.50
299	51	He, SF_6/HONO	7	2.8−9.2	8.14 ± 0.22	8.14 ± 0.60
319	63	He, SF_6/HNO_3	2	1.2−8.9	9.04 ± 0.10	9.04 ± 0.49
320	62	He, SF_6/HONO	7	1.1−7.3	8.33 ± 0.09	8.33 ± 0.45
336	63	He, SF_6,HNO_3	3	0.9−10.2	9.24 ± 0.18	9.24 ± 0.59
339	69	He, SF_6/H_2O_2	11	0.6−6.5	8.87 ± 0.03	8.87 ± 0.45
353	62	He, SF_6/HNO_3	3	2.1−8.3	9.47 ± 0.26	9.47 ± 0.70
373	61	He, SF_6/HNO_3	3	1.2−10.2	10.48 ± 0.18	10.48 ± 0.64
399	64	He, SF_6/HNO_3	2	1.2−8.6	11.22 ± 0.13	11.22 ± 0.62
400	71	He, SF_6/H_2O_2	14	1.8−11.1	10.83 ± 0.11	10.83 ± 0.58

[a] Quoted error is one standard deviations of the slope of k' vs [HCl] plot. [b] Quoted error also includes the estimated systematic error (see text) at the 95% confidence level.

TABLE 2: Rate Coefficients for the Reaction of OH with DCl, k_2, and the Relevant Experimental Conditions Used for Their Measurements[a]

temperature (K)	pressure (Torr)	$[OH]_0$ (10^{10} cm^{-3})	[DCl] (10^{15} cm^{-3})	$(k_2 \pm \sigma^b) \times 10^{13}$ (cm^3 molecule^{-1} s^{-1})	$(k_2 \pm 2\sigma^c) \times 10^{13}$ (cm^3 molecule^{-1} s^{-1})
252	103	6	1.3−10.7	1.58 ± 0.01	$1.58^{+0.08}_{-0.15}$
263	97	2	1.7−10.3	1.82 ± 0.02	$1.82^{+0.10}_{-0.17}$
286	118	2	1.6−12.0	2.25 ± 0.01	$2.25^{+0.11}_{-0.18}$
297	103	5	1.3−9.3	2.85 ± 0.04	$2.85^{+0.16}_{-0.24}$
302	117	1	1.8−11.4	2.80 ± 0.06	$2.80^{+0.18}_{-0.26}$
317	102	3	1.3−11.5	2.92 ± 0.05	$2.92^{+0.18}_{-0.26}$
321	98	4	1.2−10.9	2.72 ± 0.10	$2.72^{+0.24}_{-0.32}$
335	101	1	1.5−9.9	3.25 ± 0.04	$3.25^{+0.18}_{-0.27}$
347	99	4	1.2−13.2	3.40 ± 0.05	$3.40^{+0.20}_{-0.29}$
364	101	2	0.5−9.2	3.80 ± 0.05	$3.80^{+0.22}_{-0.32}$
387	118	1	1.3−7.8	4.81 ± 0.07	$4.81^{+0.28}_{-0.38}$

[a] Buffer gas was He. Photolysis of HNO_3 at 248 nm (from a KrF excimer laser) was used as the OH source. [b] Quoted error is one standard deviations of the slope of k′ vs [DCl] plot. [c] Quoted error also includes the estimated systematic error (see text) at the 95% confidence level. Asymmetric errors arise because the contribution of HCl, if present in the sample of DCl, only enhances the measured value.

The measured rate coefficients $k_1 - k_4$, along with the relevant experimental conditions, are listed in Tables 1−4. Various experimental checks (noted in the tables) were carried out to ensure that the rate coefficients measured in the present study were not affected by secondary reactions. Variations in the initial concentrations of OD or OH, the photolyte concentration, the linear gas flow rate through the reactor, the pressure in the reactor, and the photolysis laser fluence, did not change the measured rate coefficients. In the temperature range studied, HCl/DCl concentration measured before and after the reaction cell indicated negligible loss (possibly due to removal on the wall) of HCl/DCl inside the reactor. The quick recovery of both the 184.9 nm intensity and the measured values of k_d to their original values after turning off the reactants suggest minimal sticking or loss of HCl/DCl in the cell.

The major impurities (<10 ppmv) in HCl were N_2, O_2, CO_2, H_2, and H_2O; of these, only H_2 reacts with OH. The reaction of OH with H_2 is slow (k_{OH+H_2} at 298 K = 6.7×10^{-15} cm^3 molecule^{-1} s^{-1}).[1] Consequently, these impurities made negligible contributions to the measured rate constants. The isotopic purity of DCl is > 99%. If we assume the remaining 1% to be HCl, the measured k_2 and k_4 can be enhanced by at most 3−5% in the temperature range of our measurements.

The uncertainty in the concentration of HCl (DCl), which we conservatively estimate to be 5% at the 95% confidence level even for the lowest concentrations of HCl/DCl, is the major source of systematic error in our measurements. Estimated uncertainties due to systematic errors in concentration measurements and the probable presence of HCl impurity in the DCl sample (Tables 2 and 4) are included in the quoted errors in

TABLE 3: Rate Coefficients for the Reaction of OD with HCl, k_3, and the Relevant Experimental Conditions Used for Their Measurements[a]

temperature (K)	pressure (Torr)	$[OD]_0$ (10^{10} cm^{-3})	[HCl] (10^{15} cm^{-3})	$(k_3 \pm \sigma^b) \times 10^{13}$ (cm^3 molecule^{-1} s^{-1})	$(k_3 \pm 2\sigma^c) \times 10^{13}$ (cm^3 molecule^{-1} s^{-1})
213	63	10	1.1−7.0	6.91 ± 0.11	6.91 ± 0.41
224	66	19	1.3−7.2	6.76 ± 0.16	6.76 ± 0.47
233	64	8	1.2−7.8	6.83 ± 0.26	6.83 ± 0.62
243	57	9	1.5−11.6	7.66 ± 0.07	7.66 ± 0.41
252	64	7	1.3−7.0	7.58 ± 0.08	7.58 ± 0.41
263	90	13	0.6−7.8	7.41 ± 0.21	7.41 ± 0.56
278	65	5	1.1−8.9	7.65 ± 0.07	7.65 ± 0.41
299	63	18	1.8−8.9	8.05 ± 0.09	8.05 ± 0.44
314	65	10	1.1−4.9	9.52 ± 0.23	9.52 ± 0.66
372	65	8	1.9−8.7	10.25 ± 0.26	10.25 ± 0.73

[a] Buffer gas was He. Photolysis of DNO_3 at 248 nm (from a KrF excimer laser) was used as the OD source. [b] Quoted error is one standard deviations of the slope of k′ vs [DCl] plot. [c] Quoted error also includes the estimated systematic error (see text) at the 95% confidence level.

TABLE 4: Rate Coefficients for the Reaction of OD with DCl, k_4, and the Relevant Experimental Conditions for Their Measurements[a]

temperature (K)	pressure (Torr)	$[OD]_0$ (10^{10} cm^{-3})	[DCl] (10^{15} cm^{-3})	$(k_4 \pm \sigma^b) \times 10^{13}$ (cm^3 molecule^{-1} s^{-1})	$(k_4 \pm 2\sigma^c) \times 10^{13}$ (cm^3 molecule^{-1} s^{-1})
213	103	20	2.2−12.6	1.27 ± 0.03	$1.27^{+0.09}_{-0.15}$
224	99	13	1.0−13.5	1.41 ± 0.02	$1.41^{+0.08}_{-0.14}$
233	103	20	1.7−11.4	1.38 ± 0.03	$1.38^{+0.09}_{-0.15}$
241	98	17	0.9−16.1	1.67 ± 0.02	$1.67^{+0.11}_{-0.17}$
254	100	18	0.8−17.5	1.80 ± 0.03	$1.80^{+0.11}_{-0.18}$
262	102	13	2.1−10.3	2.03 ± 0.08	$2.03^{+0.19}_{-0.26}$
272	103	13	1.6−12.3	2.26 ± 0.06	$2.26^{+0.17}_{-0.24}$
299	51	19	1.3−11.8	2.46 ± 0.06	$2.46^{+0.17}_{-0.25}$
300	102	10	2.4−206.6	2.69 ± 0.04	$2.69^{+0.16}_{-0.24}$
314	108	25	0.2−20.6	3.13 ± 0.09	$3.13^{+0.24}_{-0.32}$
328	101	20	1.6−19.0	3.41 ± 0.05	$3.41^{+0.20}_{-0.29}$
352	105	18	2.7−14.3	4.10 ± 0.03	$4.10^{+0.22}_{-0.31}$
374	103	22	0.5−13.0	4.57 ± 0.05	$4.57^{+0.25}_{-0.35}$
401	104	17	0.4−17.7	5.20 ± 0.12	$5.20^{+0.35}_{-0.46}$

[a] Buffer gas was He. DNO_3/248 nm was used as the OD source. [b] Quoted error is one standard deviations of the slope of k′ vs [DCl] plot. [c] Quoted error also includes the estimated systematic error (see text) at the 95% confidence level. Asymmetric errors arise because the contribution of HCl, if present in the sample of DCl, only enhances the measured value.

Tables 1−4. The asymmetric error bars in Tables 2 and 4 are due to the probable impurity of HCl in DCl sample, which only enhances the measured value over the true value.

A plot of k_1 (in log scale) as a function of $1/T$ is shown in Figure 1, and the corresponding plots for $k_2 - k_4$ are depicted in Figure 2. It is clear from the figures that the conventional Arrhenius expression, $k = Ae^{-E/RT}$, does not reproduce the measured values for k_1 and k_3. Therefore, in the temperature range 200−400 K, k_1 and k_3 were fitted to a three-parameter expression of the form, $k = AT^n e^{-E/RT}$ using nonlinear least-squares analysis. The obtained parameters are shown in Tables 5 and 6. As seen in the figures, the three-parameter fits do reproduce the experimental data within the precision of the measurements. The rate coefficients for reactions of OH or OD with DCl are much smaller than those with HCl and obey Arrhenius expression, $k = Ae^{-E/RT}$ (see Figure 2). The values of A and E/R obtained from the linear least squares analyses of $\ln(k_2)$ and $\ln(k_3)$ versus $1/T$ data are shown in Table 6.

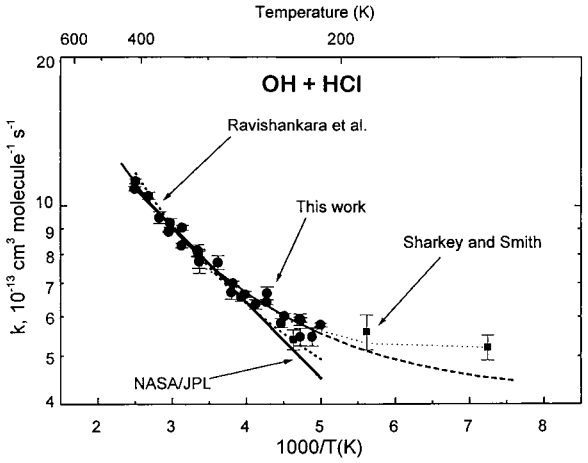

Figure 1. The plot of k_1 (on a log scale) vs $1/T$ (K): (solid circle) this work, the nonlinear fit is represented by solid line amidst the data and is extrapolated to lower temperatures as a broken thick line, (solid square) Sharkey and Smith, their nonlinear fit is represented by dotted line, (thick solid straight line) NASA/JPL evaluation;[1] (broken line) Ravishankara et al.[4]

Calculations

The potential energy surfaces for reactions 1−4 were calculated using ab initio electronic structure theory at the second-order many-body perturbation theory [MBPT(2)] and coupled-cluster singles and doubles with a perturbative triples corrections [CCSD(T)] levels. The rate constants for the four reactions were computed according to the variational transition state theory, including tunneling, using the ACESRATE program.[6] ACESRATE is an integration of the ACES III[8] electronic

TABLE 5: Comparison of Our Values of k_1 with Those from Previous Investigations[a]

T	k (10^{-13} cm^3 molecule^{-1} s^{-1})	A (cm^3 molecule^{-1} s^{-1})	$f(298)$[b]	n	$E/R \pm \Delta E/R$ (K)	T range (K)	technique	ref
298	7.8 ± 0.3	2.02×10^{-18}		2.07	−311	298−138	PLP−PLIF	5
298	8.0 ± 0.4	$(2.4 \pm 0.2) \times 10^{-12}$		0	327 ± 28	240−400	FP−RF	4
		4.5×10^{-17}		1.65	−112	240−1055		
298	8.0 ± 1.6	2.6×10^{-12}		0	350 ± 100	<400 K	evaluation	1
295(5)	7.9 ± 1.2	$(2.1 \pm 0.4) \times 10^{-12}$			285 ± 40	258−334	DF−RF	3
298	8.2 ± 1.5	$(4.6 \pm 0.3) \times 10^{-12}$		0	500 ± 60	240−295	LFP−RF	2
298	7.96 ± 0.60[c]	3.28×10^{-17}		1.66	−184	200−400	PLP−PLIF	this work
	8.0	1.7×10^{-11}	1.08	0	225 ± 20	200−298	PLP−PLIF	this work

[a] Most previous investigators expressed their rate coefficient in the conventional Arrhenius form, $k_1 = Ae^{-E/RT}$. Our results are also expressed in the 3-parameter for, $k_1 = AT^n e^{-E/RT}$, to account for the curvature in the Arrhenius plot. [b] This is the form used by data evaluations. The uncertainty at temperatures other than 298 K is given by $f(T) = f(298)\ \exp|[((E/R)((1/298)(1/T))]|$. [c] This includes estimated systematic errors at the 95% confidence level.

TABLE 6: Comparison of the Measured Rate Coefficient for the Reaction of OH Radical with DCl[a]

T	k (10^{-13} cm^3 molecule^{-1} s^{-1})	A (cm^3 molecule^{-1} s^{-1})	n	E/R (K)	T range (K)	ref
		OH + DCl (k_2)[b]				
298	3.4 ± 0.5	$(4.7) \times 10^{-12}$		780 ± 36	210−460	25
298	3.7 ± 0.22	$(3.4 \pm 0.4) \times 10^{-12}$		718 ± 32	300−700	26
298	2.52 ± 0.26	$(2.9 \pm 0.3) \times 10^{-12}$		728 ± 40	252−387	this work
		OD + HCl (k_3)				
298	8.3 ± 0.60	8.1×10^{-18}	1.85	−300	212−372	this work
		OD + DCl (k_4)				
298	2.73	$(2.5 \pm 0.2) \times 10^{-12}$		660 ± 35	213−401	this work

[a] For comparison, the summary of the rate coefficients for the reactions of OD with HCl and DCl are also listed. [b] The rate coefficients for the reaction of OH with DCl are also listed using the three-parameter form, $k = AT^n e^{-E/RT}$.

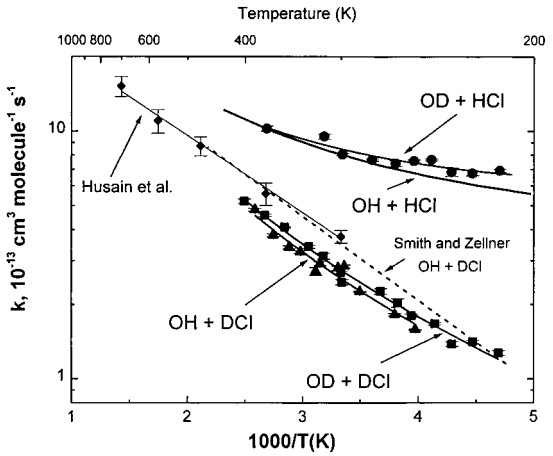

Figure 2. The plot of $k_1 - k_4$ vs $1000/T$(K). (Solid circle) OD + HCl, (solid square) OD + DCl, (solid triangle) OH + DCl, (solid line below solid circle) the data of OH + HCl. The data for OH + DCl by Husain et al.[26] (solid diamond) and those for Smith and Zellner[25] (dashed line) are also shown for comparison.

structure package and POLYRATE 7.8[9,10] The full details of the calculation are given in a previous publication.[6]

Briefly, the full energetics were calculated using MBPT(2) with the double-ζ plus polarization (D95*) basis set.[11−14] Six Cartesian *d* functions were used with this basis set. Unrestricted Hartree−Fock (UHF) reference functions were used for the open-shell species, and restricted (RHF) reference functions were used for the closed-shell species. Selected points on the potential energy surface were also computed using CCSD(T). The triple-ζ valence plus polarization (TZVP)[11,14−17] basis set was used for optimizing geometries and calculating frequencies. Final single point calculations at the CCSD(T)/TZVP geometries were done using the correlation-consistent quadruple-ζ valence plus polarization (PVQZ) basis set.[18,19] Spherical polarization functions were used with both of these basis sets. Spin contamination was monitored by the correlated spin multiplicity and found not to be significant. As an example, the value of s^2 in the MBPT(2)/D95* calculation for the OH + HCl reaction was 0.78. A summary of the stationary points on each of the potential energy surfaces is given in Table 7. This table contains three sections, one for reactants, one for products, and one for the transition state. In each section, the first row contains the total energy [CCSD(T)/PVQZ//CCSD(T)/TZVP], the next series of rows are the frequencies, and the final two rows contain both the classical energy (V_{MEP}) and the vibrationally adiabatic energy (V_a^G). The vibrationally adiabatic energy is just the classical energy plus the zero point energy for a given location on the PES. The zero of energy for both the classical and vibrationally adiabatic energy is the classical reactant energy.

The dynamics were computed using canonical variational transition state theory (CVT) (see ref 20 and citations therein) with small curvature tunneling (SCT).[21−23] The minimum energy path (MEP) was computed using MBPT(2)/D95*. The energetics computed at the MBPT(2)/D95* level were scaled using the interpolated correction (IC) method.[24] In this method the difference between a base line set of calculations, the MBPT-(2)/D95* energies, and a few points at a higher level, CCSD-(T)/PVQZ, is fit to an Eckart function. This function is used to interpolate the difference in the two curves at the other points on the path. This same method was used in the previous work[6] on reaction 1. One of the few differences between the methods reported here and the earlier results are in the interpolation methods used for calculating the effective reduced mass. In this work, POLYRATE 7.8 was interfaced with ACES II. The newer methods for computing the effective reduced mass available in POLYRATE 7.8 were used for calculating $k_1 - k_4$.

Briefly, the minimum energy path (MEP), defined to be the path of steepest descent from the transition state to reactants and products, was computed for each of the four systems using mass scaled coordinates. In each case, the MEP was computed using the method of steepest descent in the range $-0.6 < \sigma <$

TABLE 7: CCSD(T) Stationary Point Properties for Reactions 1−4[a]

properties	OH + HCl	OH + DCl	OD + HCl	OD + DCl
reactants				
total energy (hartree)	−536.023 614 113			
ν_1 (cm^{-1})	3682.7	3682.7	3009.1	2761.9
ν_2 (cm^{-1})	3009.0	2190.1	2761.9	2190.1
V_{MEP} (kcal/mol)	0.00	0.00	0.00	0.00
V_a^G (kcal/mol)	9.57	8.40	8.25	7.08
products				
total energy (hartree)	−536.052 896 235			
ν_1 (cm^{-1})	3906.1	3849.0	3849.0	2861.7
ν_2 (cm^{-1})	3786.4	2793.3	2793.3	2729.9
ν_3 (cm^{-1})	1623.4	1423.0	1423.0	1188.0
V_{MEP} (kcal/mol)	−18.37	−18.37	−18.37	−18.37
V_a^G (kcal/mol)	−5.05	−6.84	−6.84	−8.68
transition state				
total energy (hartree)	−536.019 743 558			
ν_1 (cm^{-1})	3695.3	3695.1	2690.4	2690.2
ν_2 (cm^{-1})	1387.9	1044.5	1373.9	1021.6
ν_3 (cm^{-1})	858.1	798.4	747.5	663.2
ν_4 (cm^{-1})	510.6	420.6	460.8	384.8
ν_5 (cm^{-1})	395.2	365.3	351.3	330.7
ν_6 (cm^{-1})	1413.4i	1047.5i	1411.3i	1044.7i
V_{MEP} (kcal/mol)	2.43	2.43	2.43	2.43
V_a^G (kcal/mol)	12.22	11.47	10.47	9.71

[a] Geometries and frequencies were computed using TZVP basis and the PVQZ basis set was used for the single point energies. Zero of energy is at classical reactants.

0.2 Å with a step size of 0.0008 Å and a Hessian calculation done every five steps. All vibrational degrees of freedom were computed using the harmonic approximation. Table 8 gives a summary of the computed two-level rate constants over the temperature range 200−400 K. The conventional Arrhenius expressions do not reproduce the calculated values for $k_1 - k_4$. Therefore, in the temperature range 200−400 K, each rate constant was fitted to three-parameter expression of the form $k = AT^n e^{-E/RT}$, and the obtained parameters are shown in Table 9.

Discussion

The experimental and computational k_1 values determined in this work are compared with those reported by previous investigators in Table 5 and shown in Figure 1. For temperatures from 250 to 400 K, our experimental results are in very good agreement with values from the evaluation panel and with those of Molina et al.[2] and Ravishankara et al.[4] However, at lower temperatures, k_1 from this work deviates from the extrapolations of previous studies and the NASA/JPL recommendation; e.g., our value of k_1 at 200 K is ∼25% higher than the NASA/JPL recommendation and in good agreement with the interpolated value of Sharkey and Smith.[5] The fit to our data (Figure 1) agrees with the data of Sharkey and Smith down to 185 K. However, it should be noted that Sharkey and Smith report only four measurements between 138 and 298 K. The k_1 values reported by Sharkey and Smith were the same, within their measurement uncertainties, from 216 down to 138 K. One important feature to note in the plots (Figure 1) is that the two-parameter Arrhenius expression predicts rate coefficients that are progressively lower than the measured quantities.

Figure 3 compares the measured and calculated values of k_1. In the temperature range $250 < T < 353$ K, the calculated values of k_1 agree with the measurements to within ∼10%. At temperatures between 200 and 250 K, the computed rate constants are higher, but agree within ∼30% with the measured values. Between 353 and 400 K, the computed rates are up to 17% lower than the measured values.

The 298 K rate coefficients for the reaction of OH with DCl (k_2) are compared with the previous measurements of Smith and Zellner,[25] and Husain et al.[26] in Figure 2 and Table 6. The computed values are given in Table 8. Smith and Zellner's measured value of $(3.4 \pm 0.5) \times 10^{-13}$ cm^3 $molecule^{-1}$ s^{-1} and Husain et al.'s value of $(3.7 \pm 0.22) \times 10^{-13}$ cm^3 $molecule^{-1}$ s^{-1} are both higher than our measured value of $(2.52 \pm 0.19) \times 10^{-13}$ cm^3 $molecule^{-1}$ s^{-1} or our computed value of 2.41×10^{-13} cm^3 $molecule^{-1}$ s^{-1} at 298 K. However, the activation energies agree with our measured value (see Table 6). The significantly higher k_2 values could be due to the conversion of DCl to HCl via exchange with water vapor, which was used as the OH precursor in the experiments of Smith and Zellner as well as Husain et al. If such an exchange occurred, the agreement in E/R may be fortuitous. As described above, we took great care to minimize isotopic exchange; therefore, we believe that our values are correct.

In Figure 4, the ratios, k_1/k_2 and k_3/k_4, are plotted to show the primary kinetic isotope effect, PKIE, for reaction with both

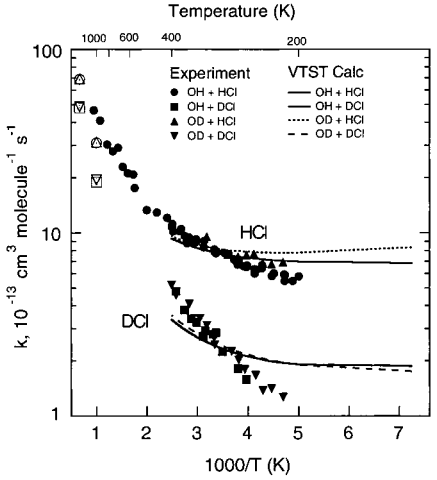

Figure 3. Comparison of the measured and calculated values of $k_1 - k_4$ as a function of temperature. The values of k_1 above 400 K are from ref 4. The calculated values between 200 and 400 K are represented as curves and the discrete values calculated at a few higher temperatures are also shown as open circles (k_1), open squares (k_2), open triangles (k_3), and open inverted triangle (k_4).

TABLE 8: Forward CVT/SCT//MBPT(2)/D95*//CCSD(T)/PVQZ Two-level Rate Constants for OH + HCl, OH + DCl, OD + HCl, and OD + DCl Reactions and the Corresponding Experimental Value[a]

	OH + HCl (k_1)		OH + DCl (k_2)		OD + HCl (k_3)		OD + DCl (k_4)	
T (K)	exptl	CVT/SCT	exptl	CVT/SCT	exptl	CVT/SCT	exptl	CVT/SCT
200	5.78	6.97		1.91		7.80		1.90
205	5.47	6.99		1.93		7.79		1.92
211	5.91	7.03		1.94		7.79		1.95
212	5.78	7.03		1.95		7.79		1.95
213		7.04		1.95	6.91	7.79	1.27	1.96
224	5.83	7.11		1.99	6.76	7.80	1.41	2.01
233		7.18		2.03	6.83	7.82	1.38	2.06
234	6.55	7.18		2.04		7.82		2.07
241		7.24		2.07		7.85	1.67	2.11
243	6.35	7.26		2.08	7.66	7.86		2.12
251	6.65	7.32		2.12		7.89		2.17
252		7.33	1.58	2.12	7.58	7.90		2.18
254	6.57	7.35		2.13		7.91	1.80	2.19
262	7.00	7.42		2.18		7.95	2.03	2.24
263	6.71	7.43	1.82	2.18	7.41	7.96		2.25
272		7.52		2.24		8.02	2.26	2.31
277	7.70	7.57		2.27		8.06		2.35
278		7.58		2.27	7.65	8.06		2.35
286		7.67	2.25	2.33		8.13		2.41
297	7.74	7.79	2.85	2.40		8.23		2.50
298		7.80		2.41		8.23		2.51
299	8.09	7.82		2.42	8.05	8.24	2.46	2.52
300		7.83		2.42		8.25	2.69	2.53
302		7.85	2.80	2.44		8.27		2.54
314		8.00		2.53	9.52	8.40	3.13	2.64
317		8.04	2.92	2.55		8.43		2.67
319	9.04	8.06		2.57		8.45		2.69
320	8.33	8.07		2.58		8.46		2.70
321		8.09	2.72	2.58		8.47		2.70
328		8.18		2.64		8.55	3.41	2.77
335		8.28	3.25	2.70		8.64		2.83
336	9.24	8.29		2.71		8.65		2.84
339	8.87	8.33		2.74		8.69		2.87
347		8.45	3.40	2.81		8.79		2.95
352		8.52		2.85		8.86	4.10	3.00
364		8.70	3.80	2.97		9.02		3.12
372		8.83		3.05	10.3	9.14		3.21
373	10.5	8.84		3.06		9.15		3.22
374		8.86		3.07		9.17	4.57	3.23
387		9.07	4.81	3.20		9.37		3.38
399	11.2	9.28		3.33		9.56		3.52
400	10.8	9.29		3.34		9.58		3.53
401		9.31		3.36		9.60	5.20	3.54

[a] All rate coefficients are in units of 10^{-13} cm^3 molecule^{-1} s^{-1}.

TABLE 9: Three-parameter $k = AT^n e^{-E/RT}$ Fits to the CVT/SCT Computed Rate Constants for the OH + HCl Reaction and the Primary and Secondary Isotope Effects over the Temperature Range 200−400 K

reaction	A (cm^3 molecule^{-1} s^{-1})	n	E/R (K)
OH + HCl	1.49×10^{-16}	1.35	−262
OH + DCl	9.04×10^{-20}	2.34	−429
OD + HCl	1.01×10^{-16}	1.40	−309
OD + DCl	1.64×10^{-19}	2.27	−385

OH and OD. It is seen that the PKIE for reaction of OD is slightly higher than the reaction of OH. The higher measured and computed values of k_1 and k_3 compared to k_2 and k_4 (approximately a factor of 3) indicate that the reactions (1−4) proceed via an abstraction mechanism in which the OH/OD radical abstracts the hydrogen/deuterium atom from HCl/DCl. We attribute the faster rate for the reactions with HCl over those of DCl to the primary kinetic isotope effect. The curved Arrhenius plots for k_1 and k_3 compared to those for k_2 and k_4 suggest that at lower temperature H atom tunneling becomes significant in reactions 1 and 3.

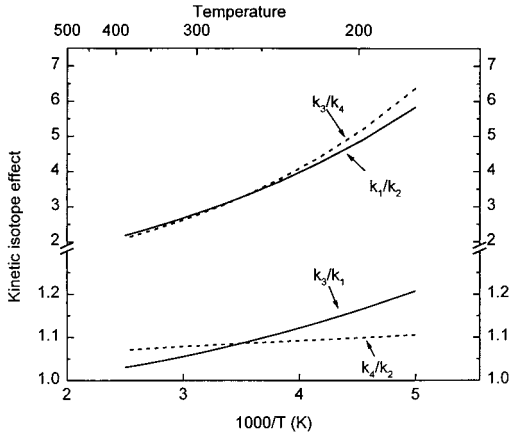

Figure 4. The plot of ratios of measured rate coefficients to show the primary (k_1/k_2 and k_3/k_4) and secondary kinetic isotope effect (k_3/k_1 and k_4/k_2) vs $1/T$.

The secondary kinetic isotope effect, (i.e., $k_3 > k_1$ and $k_4 > k_2$) is detectable for $T < 298$ K (see Tables 1- 6 and Figure 2). The ratios k_3/k_1 and k_4/k_2 versus $1/T$ are plotted in Figure 4. In studying reaction 2, HNO_3 was used as the OH precursor. If there had been an exchange between HNO_3 and DCl, HCl would have formed. This would increase the measured rate constant compared to that with pure DCl. Thus, if there was an exchange one would measure $k_2 > k_4$. However, the reverse was observed, i.e., $k_4 > k_2$ (see Figure 4). Similarly, if there was an exchange, we would have observed $k_1 > k_3$. Again we observed $k_1 < k_3$. Moreover, the concentrations of HCl and DCl were measured in the same way for determining the rate coefficients. Therefore, we believe the secondary kinetic isotope effect observed in our experiments is real and not an experimental artifact. Such a secondary kinetic isotope effect has been observed[7] for OD reaction with H_2 and CH_4. Results of conventional transition state theory calculations performed for the reaction of OD with CH_4 support this observation. The OD−HCl transition state has lower frequency modes than OH−HCl transition state, thus make the OD−HCl reaction a little faster than the OH−HCl reaction. The difference between the zero point energy of OD and the influence of D atom on several modes in the transition state results in a reduction of the barrier height of OD−HCl transition state than the OH−HCl transition state. This results in a higher rate constant for OD reactions than that for OH reactions. Similarly, calculations performed here show that the effective barrier (V_a^G), as given in Table 7, is highest for reaction 1 (12.22 kcal/mol), then decreases for reaction 2 (11.47 kcal/mol) and reaction 3 (10.47 kcal/mol), and is the lowest for reaction 4 (9.71 kcal/mol).

To better understand the differences in rate coefficients for reactions 1 and 3 and reactions 2 and 4 we present a factor analysis of the kinetic isotope effects (KIE's).[27] The theoretical expression for the ratio of the CVT/SCT rate constants may be factored into five components associated with quantal effects on reaction-coordinate motion: tunneling (TUN), vibrations (VIB), rotation (ROT), translational motion (TRANS), and potential energy along the minimum-energy path (POT). Table 10 shows this breakdown for the room-temperature primary and secondary isotope effects. This table shows that the dominant contribution to the primary isotope effects is vibration and rotation. For the secondary isotope effects, tunneling also becomes important. In all cases, the translational and potential energy contributions are negligible. It is clear that tunneling

TABLE 10: Factors for the Kinetic Isotope Effects (KIE) at 298 K

	TUN	VIB	ROT	POT	TRANS	KIE (calculated)	KIE (measured)
k_1/k_2	0.99	1.78	1.78	1.02	1.01	3.25	3.08
k_3/k_4	1.01	1.75	1.82	1.02	1.01	3.30	3.06
k_3/k_1	0.67	2.25	0.75	1.00	0.94	1.06	1.08
k_4/k_2	0.66	2.30	0.73	1.00	0.94	1.04	1.08

correction is one of the major source of discrepancy between measured and computed rate constants.

Atmospheric Implications

The atmospheric impact of the change in k_1 was examined using the Garcia-Solomon two-dimensional dynamical-chemical-radiative model (see refs 28 and 29 and citations therein). The model was run for the 1975−1997 period using both the recommendations of DeMore et al.[1] (called NASA/JPL-97) and the three-parameter fit to k_1 measured here. The results corresponding to chlorine of the 1990s are presented here.

The rate coefficient for the reaction of OH with HCl reported here is higher than that recommended by DeMore et al.[1] at stratospheric temperatures. The difference is > 20% below 200 K, while it is about 10% at 220 K and 5% at 240 K. Thus, significant changes in active chlorine (and thus ClO) may be expected in the lower stratosphere, especially during winter and spring when temperatures are coldest. However, the modeled changes in ClO are only 5−10% in the lower stratosphere. While still large, several factors mitigate the expected large effect due to the higher value of k_1. First, at temperatures below ∼205 K direct heterogeneous removal of HCl dominates the chlorine partitioning. Second, the abundance of OH is greatly reduced when temperatures are as low as 200 K due to the slowing down of other temperature dependent reactions and also due to the low light levels (higher solar zenith angles) which typically accompany the coldest temperatures. Finally, since HCl is relatively long-lived in the lower stratosphere (with a lifetime on the order of weeks), the chemical changes must compete with transport from above.

The local changes in O_3 due to these rate constant change for 1990 chlorine levels in the lower stratosphere are on the order of 0.5−2%, corresponding to a 1−3 dobson unit change in column O_3. The reduced effect on O_3 (compared with ClO) is due to the relatively small (10−30%) amount that chlorine contributes to the total ozone catalytic loss rate in the lower stratosphere. Larger chlorine-induced ozone loss under certain conditions (e.g., Antarctic ozone hole) is due to much larger changes in ClO abundance caused by heterogeneous activation. The modeled changes in ozone are larger in winter and spring by a factor of about 0.5−1 compared with summer and fall. These changes in ozone, though relatively modest, show that modelers in future studies should adopt the reported rate coefficient.

References and Notes

(1) DeMore, W. B.; Sander, S. P.; Golden, D. M.; Hampson, R. F.; Kurylo, M. J.; Howard, C. J.; Ravishankara, A. R.; Kolb, C. E.; Molina, M. J. *Chemical Kinetics and Photochemical Data for Use in Stratospheric Modeling*; JPL Publication 97-4; Jet Propulsion Laboratory: Pasadena, CA, 1997.

(2) Molina, M. J.; Molina, L. T.; Smith, C. A. *Int. J. Chem. Kinet.* **1984**, *16*, 1151−1160.

(3) Keyser, L. F. *J. Phys. Chem.* **1984**, *88*, 4750−4758.

(4) Ravishankara, A. R.; Wine, P. H.; Wells, J. R.; Thompson, R. L. *Int. J. Chem. Kinet.* **1985**, *17*, 1281−1297.

(5) Sharkey, P.; Smith, I. W. M. *J. Chem. Soc., Faraday Trans.* **1993**, *89*, 631−638.

(6) Steckler, R.; Thurman, G. M.; Watts, J. D.; Bartlett, R. J. *J. Chem. Phys.* **1997**, *106*, 3926−3933.

(7) Gierczak, T.; Talukdar, R. K.; Herndon, S. C.; Vaghjiani, G. L.; Ravishankara, A. R. *J. Phys. Chem.* **1997**, *101*, 3125−3134.

(8) Stanton, J. F.; Gauss, J.; Watts, J. D.; Nooijen, M.; Oliphant, N.; Perera, S. A.; Szalay, P. G.; Lauderdale, W. J.; Gwaltney, S. R.; Beck, S.; Balková, A.; Bernholdt, D. E.; Baeck, K.-K.; Sekino, H.; Huber, C.; Bartlett, R. J. ACES II, program product of the Quantum Theory Project, University of Florida. Integral packages included are VMOL (J. Almlof and P. R. Taylor); VPROPS (P. R. Taylor); and ABACUS (T. Helgaker, H. J. Aa. Jensen, P. Jorgensen, J. Olsen, and P. R. Taylor); Quantum Theory Project, University of Florida: Gainesville, FL, 1994.

(9) Steckler, R.; Hu, W.-P.; Liu, Y.-P.; Lynch, G. C.; Garrett, B. C.; Isaacson, A. D.; Melissas, V. S.; Lu, D.-h.; Troung, T. N.; Rai, S. N.; Hancock, G. C.; Lauderdale, J. G.; Joseph, T.; Truhlar, D. G. *Comput. Phys. Commun.* **1995**, *88*, 341−343.

(10) Corchado, J. C.; Chuang, Y.-Y.; Fast, P. L.; Villa, J.; Coitino, E. L.; Hu, W.-P.; Y.-P. Liu; Lynch, G. C.; Nguyen, K. A.; Jackels, C. F.; Gu, M. Z.; Rossi, I.; Clayton, S.; Melissas, V. S.; Steckler, R.; Garrett, B. C.; Isaacson, A. D.; Truhlar, D. G. *POLYRATE*, Version 7.8; University of Minnesota: Minneapolis, 1997.

(11) Huzinaga, S. *J. Chem. Phys.* **1965**, *42*, 1293.

(12) Dunning, T. H., Jr. *J. Chem. Phys.* **1970**, *53*, 2823−33.

(13) Dunning, T. H., Jr.; Hay, P. J.. In *Methods of Electronic Structure Theory*; Schaefer, H. F., III, Ed.; Plenum: New York, 1977.

(14) Huzinaga, S. Approximate Atomic Functions II; Department of Chemistry Report, University of Alberta: Alberta, Canada, 1971.

(15) Dunning, T. H., Jr. *J. Chem. Phys.* **1971**, *55*, 716.

(16) Ahlrichs, R.; Taylor, P. R. *J. Chim. Phys.* **1981**, *78*, 315−24.

(17) McLean, A. D.; Chandler, G. S. *J. Chem. Phys.* **1980**, *72*, 5639−48.

(18) Dunning, T. H., Jr. *J. Chem. Phys.* **1989**, *90*, 1007.

(19) Woon, D. E.; Dunning, T. H., Jr. *J. Chem. Phys.* **1993**, *98*, 1358.

(20) Truhlar, D. G.; Brown, F. B.; Steckler, R.; Isaacson, A. D. The Representation and Use of Potential Energy Surfaces in the Wide Vicinity of a Reaction Path for Dynamics Calculations on Polyatomic Reactions. In *The Theory of Chemical Reaction Dynamics*; Clary, D. C., Ed.; D. Reidel: Dordrecht, Holland, 1986; pp 285−329.

(21) Lu, D.-h.; Truong, T. N.; Melissas, V. S.; Lynch, G. C.; Liu, Y.-P.; Barrett, B. C.; Steckler, R.; Isaacson, A. D.; Rai, S. N.; Hancock, G. C.; Lauderdale, J. G.; Joseph, T.; Truhlar, D. G. *Comput. Phys. Comm.* **1992**, *71*, 235−262.

(22) Liu, Y.-P.; Lynch, G. C.; Truong, T. N.; Lu, D.-h.; Truhlar, D. G.; Garrett, B. C. *J. Am. Chem. Soc.* **1993**, *115*, 2408.

(23) Skodje, R. T.; Truhlar, D. G.; Garrett, B. C. *J. Phys. Chem.* **1981**, *85*, 3019−3023.

(24) Hu, W.-P.; Liu, Y.-P.; Truhlar, D. G. *J. Chem. Soc., Faraday Trans. 1* **1994**, *90*, 1715−1725.

(25) Smith, I. W. M.; Zellner, R. *J. Chem. Soc., Faraday Trans. 2* **1974**, *70*, 1045−1056.

(26) Husain, D.; Plane, J. M. C.; Xiang, C. C. *J. Chem. Soc., Faraday Trans. 2* **1984**, *80*, 713−728.

(27) Tucker, S. C.; Truhlar, D. G.; Garrett, B. C.; Isaacson, A. D. *J. Chem. Phys.* **1985**, *82*, 4102.

(28) Garcia, R. R.; Stordal, F.; Solomon, S.; Kiehl, J. T. *J. Geophys. Res.* **1992**, *97*, 12, 967−12, 991.

(29) Garcia, R. R.; Solomon, S. *J. Geophys. Res.* **1994**, *99*, 12, 937−12, 951.